tvst

Article

Stromal Nerve Imaging and Tracking Using Micro-Optical Coherence Tomography

Carolin Elhardt[1,2], Christian M. Wertheimer[1,2,*], Andreas Wartak[1,3,*], Jie Zhao[1,3], Hui Min Leung[1,3], Stefan A. Kassumeh[1,2], Biwei Yin[1,3], Guillermo J. Tearney[1,3,4,5,], and Reginald Birngruber[1,6,**]**

[1] Wellman Center for Photomedicine, Massachusetts General Hospital, Boston, MA, USA
[2] Department of Ophthalmology, Ludwig-Maximilians-University Munich, Munich, Germany
[3] Harvard Medical School, Boston, MA, USA
[4] Harvard-MIT Division of Health Sciences and Technology, Cambridge, MA, USA
[5] Department of Pathology, Harvard Medical School and Massachusetts General Hospital, Boston, MA, USA
[6] Institute of Biomedical Optics, University of Lübeck, Lübeck, Germany

Correspondence: Carolin Elhardt, Wellman Center for Photomedicine, 40 Blossom St, Boston, MA 02114, USA. e-mail: Elhardt@med.uni-muenchen.de

Received: October 2, 2019
Accepted: January 12, 2020
Published: April 15, 2020

Keywords: optical coherence tomography; micro-OCT; imaging; corneal nerves; diabetes

Citation: Elhardt C, Wertheimer CM, Wartak A, Zhao J, Leung HM, Kassumeh SA, Yin B, Tearney GJ, Birngruber R. Stromal nerve imaging and tracking using micro-optical coherence tomography. Trans Vis Sci Tech. 2020;9(5):6, https://doi.org/10.1167/tvst.9.5.6

Purpose: To image, track and map the nerve fiber distribution in excised rabbit corneas over the entire stromal thickness using micro-optical coherence tomography (µOCT) to develop a screening tool for early peripheral neuropathy.

Methods: Excised rabbit corneas were consecutively imaged by a custom-designed µOCT prototype and a commercial laser scanning fluorescence confocal microscope. The µOCT images with a field of view of approximately 1 × 1 mm were recorded with axial and transverse resolutions of approximately 1 µm and approximately 4 µm, respectively. In the volumetric µOCT image data, network maps of hyper-reflective, branched structures traversing different stromal compartments were segmented using semiautomatic image processing algorithms. Furthermore, the same corneas received βIII-tubulin antibody immunostaining before digital confocal microscopy, and a comparison between µOCT image data and immunohistochemistry analysis was performed to validate the nerval origin of the tracked network structures.

Results: Semiautomatic tracing of the nerves with a high range of different thicknesses was possible through the whole corneal volumes, creating a skeleton of the traced nerves. There was a good conformity between the hyper-reflective structures in the µOCT data and the stained nerval structures in the immunohistochemistry data.

Conclusions: This article demonstrates nerval imaging and tracking as well as a spatial correlation between µOCT and a fluorescence corneal nerve standard for larger nerves throughout the full thickness of the cornea ex vivo.

Translational Relevance: Owing to its advantageous properties, µOCT may become useful as a noncontact method for assessing nerval structures in humans to screen for early peripheral neuropathy.

Introduction

Peripheral neuropathy (PN) is a common morbid condition in a wide range of medical diseases and disorders, including diabetes and autoimmune, hereditary, and infectious diseases.[1–5] Especially diabetic peripheral polyneuropathy is an important condition that affects 30% to 50% of patients with diabetes.[3] Potentially severe symptoms, such as neuropathic pain, may result in a substantial impact on the quality of life of patients.[6] In general, peripheral nerves are damaged systemically owing to advanced glycosylation products that accumulate in the nerves in the setting of high blood glucose levels. Early detection of peripheral nerve changes could possibly enable intensification of blood glucose–lowering treatment that could halt PN progression. Clinical trials have shown that

the morphologic repair of corneal nerve fibers may be detected when glycemic control improves.[7]

However, early diagnosis of PN has proven to be challenging to date. Nerval degeneration starts in the most peripheral nerval branches,[1] manifesting as a decrease in fiber and branch density[8] and changes in corneal nerve tortuosity.[9] These features are challenging to measure or visualize in most tissues, owing to the small size of peripheral nerves and the lack of contrast for most imaging modalities. Possible clinical examinations include vibration testing with tuning forks, light touch perception with monofilaments, superficial pain perception, testing of ankle deep tendon reflexes, electromyography, and nerve conduction studies.[10,11] However, these methods primarily test the functionality of larger nerve fibers. One promising approach for the early diagnosis of PN is to image the nerves directly to identify abnormalities. Peripheral nerve imaging can be performed, for example, using magnetic resonance imaging, diffusion tensor imaging, ultrasound examination, and positron emission tomography; however, these techniques lack resolution to image small nerve fibers or do not image the nerves directly.[12,13]

There is one exceptional tissue that allows the visualization of incipient denervation by light microscopy because of its good accessibility and optical transparency: the cornea.[14] It is innervated by the ophthalmic division of the trigeminal nerve. Nerve bundles enter the cornea peripherally before subdividing into a network of several smaller branches that mostly extend parallel to the corneal surfaces. The nerve density is reported to be highest in anterior and mid stroma. However, the nerve branches take a 90° turn toward the Bowman's membrane before penetrating it to form the sub-basal plexus and superficial nerve endings. All three described corneal networks—midstromal, sub-basal, and epithelial—are supplied by the corneal stroma.[15,16]

Clinical evaluation of corneal nerves is currently performed using commercially available in vivo confocal microscopy (IVCM).[16–18] It was demonstrated to be superior to six other techniques for detecting the early onset of diabetic PN by imaging small nerve fibers[19] and reported to enable determination of PN prognosis.[20] Furthermore, corneal nerve fiber length, measured in length per volume, was proposed to be a useful parameter to detect changes associated with diabetic polyneuropathy.[21] Being significantly lower in diabetes patients, fiber length is considered a good marker for peripheral nerve damage[22] as well as also diabetic retinopathy.[23]

Confocal microscopy provides high lateral resolutions of just below 1 µm. However, the use of IVCM as a standard-of-care PN screening procedure has been hindered owing to several technical limitations: (i) its small field of view (FoV) of approximately 400 µm × 400 µm, (ii) its capacity to only generate transverse or en face images, one depth at a time, and (iii) its requirement that physical contact be maintained between the microscope's objective lens and the patient's corneal surface, thus being at least minimally invasive. These limitations increase the time and complexity of the procedure by requiring stitching of several image tiles, demand expert operation, and frequently cause discomfort to the patient.

Recently, a cross-sectional reflectance microscopy technique called optical coherence tomography (OCT) has been reported to enable imaging of corneal nerval structures in vivo.[24] In comparison with IVCM, OCT offers high-speed, depth-resolved, and noninvasive volumetric imaging.[25] Clinical anterior segment OCTs with axial and transverse resolutions of approximately 7 to 10 µm and approximately 15 to 25 µm lack the resolution to resolve smaller corneal nerves. OCT technology advances, such as full-field OCT [26] or micro-OCT (µOCT),[27] with near isotropic 1 to 2 µm resolutions, have recently been shown to be capable of imaging small corneal nerve structure details, especially within the sub-basal plexus.[24,28–30]

In this article, we introduce µOCT for high-resolution nerval imaging within the entire corneal stroma to validate µOCT nerve imaging as a screening tool for early PN, for example in patients with diabetes.

Methods

Imaging

Imaging was conducted using a bench-top spectral domain µOCT instrument. The imaging setup was already presented elsewhere where the name µOCT originates from, with regard to its high micrometer resolution.[27,31,32] In short, the system featured a supercontinuum light source (NKT Photonics, Inc., Birkerød, Denmark) and operated at a central wavelength of 800 nm with a bandwidth of ±150 nm used for imaging. The 8192-pixel line-scan camera (Basler AG, Ahrensburg, Germany) in the spectrometer was operated at 20 kHz, and volumetric scans were acquired over a FoV of 1 × 1 mm at a sampling of 512 × 512 pixels. These parameters resulted in an acquisition time of approximately 13 seconds per volume and an illumination power of approximately 20 mW at the sample. The axial and transverse resolutions of the instrument were approximately 1 µm and approximately 4 µm in tissue, respectively.

After standard spectral domain μOCT image reconstruction, all additional image processing was carried out in the open source software ImageJ (ImageJ 1.50c4, National Institutes of Health, Bethesda, MD).[33] The software plugin Simple Neurite Tracer[34] was used for tracking and marking corneal nerve structures throughout a corneal μOCT volume. This plugin allows for the semiautomatic marking of structures across neighboring B-scans on the basis of image segmentation, eventually enabling three-dimensional (3D) tracing.

A commercially available automated laser scanning fluorescence confocal microscope (FCM; Fluoview FV1000 coupled IX81, Olympus, Tokyo, Japan) was used for image acquisition of the entire stained cornea. A 4× objective (0.16 NA) and the multiarea time lapse function were applied for large area whole cornea tile images. For dye excitation, light at 635 nm was used and the fluorescent emission was detected from 660 to 730 nm.

Sample Preparation and Immunohistochemistry

The study was performed on excised rabbit eyes owing to their similar physiologic corneal features in relation to humans. All study procedures were approved by the Institutional Animal Care and Use Committee (exempt ID: 2017N000222) of Massachusetts General Hospital (Boston, MA) and adhered to the ARVO Animal Statement. Mature fresh New Zealand White rabbit cadaver globes were used for μOCT imaging within 24 hours of the animal's death. For transport, they were kept in a 4°C balanced salt solution. To perform corneal imaging, corneoscleral discs of a diameter of approximately 17 mm were separated from the rest of the globes using keratoplasty scissors (Katena, Denville, NJ). The discs were placed in phosphate-buffered saline (PBS; Fisher Bioreagents, Geel, Belgium) containing 20% w/v Dextran (MW 450,000–600,000; Sigma, St. Louis, MO) for a minimum of 30 minutes, for them to dehydrate to their regular corneal thickness. Before imaging, the discs were mounted onto a custom-designed anterior segment chamber with a diameter of 13.75 mm to prevent distortion of the natural rabbit cornea curvature. A water column was connected to the chamber to generate normal eye pressure of 18 mm Hg. To avoid corneal desiccation, their outside surface was sprinkled with PBS containing 20% w/v Dextran between μOCT recordings.

Indirect immunohistochemistry of the corneal nerves was performed using a protocol of a βIII-tubulin antibody staining,[35] slightly adjusted to the corneal model. The corneas were washed in PBS before being fixed in a 4% solution of paraformaldehyde (Sigma-Aldrich) in distilled water for 2 hours at 4°C, followed by rehydration in PBS at 4°C overnight.

To achieve antigen unmasking and axon membrane permeabilization, the corneas were washed at gentle rotation in PBS with 1% Triton X-100 (Electron Microscopy Science, Hatfield, PA) three times for 20 minutes each. To inhibit unspecific staining, the corneas were blocked two times for 60 minutes and two times for 5 minutes in a blocking solution (0.25% casein in PBS, containing stabilizing protein and 0.015 mol/L sodium azide; Agilent #X090930-2, Santa Clara, CA) at room temperature at gentle rotation. Subsequently, the corneas were cut at four locations from the periphery toward the center to enable flattening. The epitopes marking was performed using a mouse anti–βIII-tubulin antibody (Cat# 801202, Biolegend, San Diego, CA, USA), diluted 1:1000 in blocking solution, for 4 days at 4°C and gentle rotation. Thereafter, they were gently rotated at room temperature for 30 minutes and then washed three times for 60 minutes in blocking solution and three times for 10 minutes in PBS 1% Triton X-100 at gentle rotation. An AlexaFluor 647 labeled goat antimouse antibody (Cat# 21235, Thermo Fisher Life Technologies, Carlsbad, CA) 1:200 diluted, diluted in blocking buffer, was applied as secondary antibody for 2 days at 4°C and gentle rotation in a dark environment. After antibody labeling, three times washing for 30 minutes in PBS 1% Triton X-100 and three times for 15 minutes in PBS in the dark at gentle rotation was performed. Finally, the corneas were mounted in between a slide and cover glass using ProLong Gold Antifade Mountant with 4′,6-diamidin-2-phenylindol (Cat# 36935, Thermo Fisher Scientific, Waltham, MA) and the cover glass sealed with transparent nail polish.

Results

The acquired volumetric μOCT datasets featured hyper-reflective branching structures of different caliber throughout the stroma. Figure 1 depicts a representative image data of an ex vivo rabbit cornea, clearly illustrating the stromal nerve network. Figures 1B and 1C present en face projections (approximately 15 μm in depth) of different caliber structures. A large Y-shaped nerval bifurcation in the midstromal region surrounded by keratocytes is presented in Figure 1B. This figure merges two neighboring en face projections from consecutively acquired data

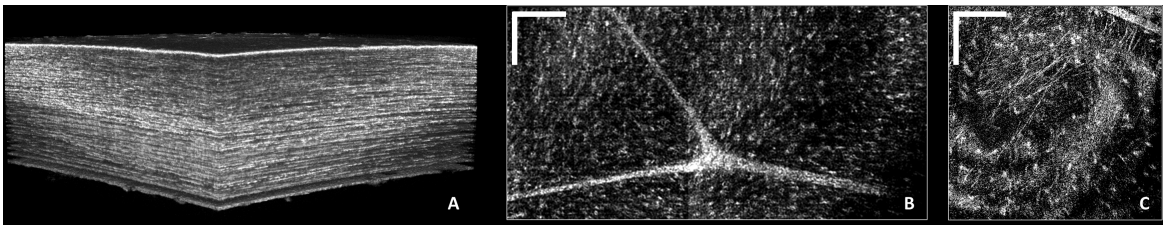

Fig. 1. Representative ex vivo rabbit corneal µOCT image data. (A) Three-dimensional rendered volume dataset. (B) Large corneal nerve bifurcation in the anterior to mid stromal region surrounded by keratocytes (two stitched datasets of consecutive recordings). (C) Anterior stroma presenting a network of thin corneal nerve fibers (as well as a larger nerve in the top right corner) and uniformly distributed keratocytes. Images (B) and (C) are averaged over approximately 15 µm in depth. Scale bar = 250 µm.

sets. The anterior stromal nerve network (thin hyper-reflective line structures and a thick structure in the top right corner of the image) as well as uniformly distributed keratocytes are visible in Figure 1C.

Nerve Validation

The assumption of the nerval origin of the hyper-reflective structures described in Figures 1B and 1C was made with regard to their elongated shape, branching pattern, and the lack of any known structurally similar constituent within the stromal architecture. To confirm their nerval origin, an image comparison between FCM and µOCT was performed (Fig. 2). The same cornea was consecutively imaged using both modalities. As a reference, to enable retrieval of the exact corneal location of the recorded µOCT data sets with regards to the FCM image, a thin wire was stitched into the corneal stroma (indicated by white arrow heads in Fig. 2A and 2C). The FCM data show a common corneal nerve fiber distribution, where the larger nerves in the limbal regions extend toward the center, constantly branching and, thus, decreasing in thickness (Fig. 2B), integrated over entire corneal thickness. However, nerval structures beyond the third or fourth branching generation are difficult to assess or invisible, owing to a significantly reduced fiber thickness. Therefore, only the largest visible nerve structures in µOCT data could be addressed for image comparison. Figure 2C presents an overlay of four en face µOCT images over a zoom-in of Figure 2B. In addition, the four regions of interest are presented below the overlay in a side-by-side comparison between µOCT and FCM (Fig. 2D). The hyper-reflective structures in the µOCT data match most of the green nerval structures indicated in the FCM data. However, not all of the stained nerves in every respective region of interest also appear to be present in the µOCT data. This lack of correspondence can be explained by the fact that the µOCT en face sections are only depth integrated over a range of 15 to 20 µm, whereas the FCM data were integrated over the whole corneal thickness. Slight deviations in shape as apparent in region of interest 4 are attributed to differences in corneal curvature at image acquisition (anterior segment mount vs. flat mount).

Three-Dimensional Corneal Nerve Tracking

The application of the imaging software plugin Simple Neurite Tracer allowed semiautomatic tracing of the nerves through the whole corneal volumes. Figure 3A shows a corneal 3D-rendered volume dataset. The semiautomatic traces of the whole volume are depicted as en face (Fig. 3B) and cross-sectional (Fig. 3C) plane nerve trace skeletons integrated over the entire corneal thickness, respectively, over the entire lateral extension of scan. A rotation of the traced nerve skeleton is presented in the Supplementary Movie S1 to facilitate 3D perception. Figure 3D presents traced nerve structures, overlaid in magenta, in a single representative en face plane. A zoom-in of this region is displayed in Figure 3E, providing a close-up of the tracking procedure. To enable comparison, the same region is shown in Figure 3F as untracked raw intensity en face plane.

Discussion

In this study, we demonstrate visualization and semiautomatic tracking of the corneal nerval network by µOCT. Excised rabbit corneas were imaged using a bench-top µOCT instrument, and the nerval origin of the observed hyper-reflective linear structures was validated using selective βIII-tubulin antibody staining and FCM. Finally, the stromal nerve fiber distribution was assessed via semiautomatic tracking.

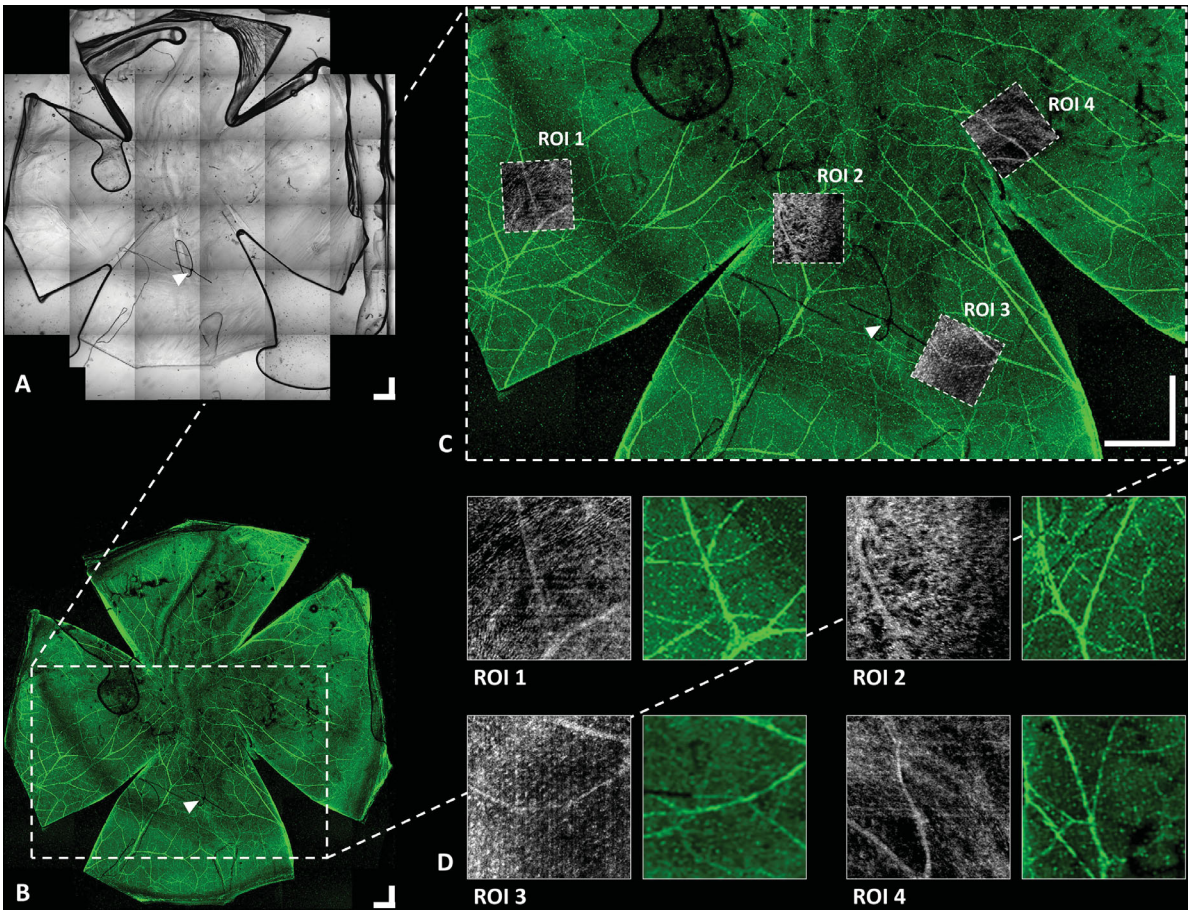

Fig. 2. Comparison of flat-mounted βIII-tubulin antibody-immunostained FCM versus an anterior segment model mounted, untreated µOCT of the same cornea, to confirm the nerval origin of the hyper-reflective fibrous structures in the µOCT scans. (A) Normal depth integrated FCM image of a flat-mounted cornea. (B) Green fluorescent depth integrated FCM image of a flat-mounted cornea. (C) Zoom-in of (B) with en face overlays of µOCT data sets at respective large corneal nerve structures (regions of interest 1–4). (D) Side-by-side comparison of regions of interest 1 to 4 between µOCT and FCM. Scale bar = 1 mm.

Good knowledge of the corneal nerve network structure has been provided by electron microscopy,[36] histochemical,[37] immunohistochemical,[35] and confocal microscopy studies. Our µOCT results are in accordance with the previous described findings and our confocal immunohistochemistry study on the same tissue.

IVCM is the primary imaging modality for corneal nerve visualization.[16–18] Being available for more than 20 years and having commercially available platforms on the market, IVCM is currently clearly a step ahead of OCT. Its advantageous high resolution enables outstanding image quality at the cellular level—even in vivo.[38] Nevertheless, owing to the aforementioned technical shortcomings, as of yet, IVCM has not become a standard method in daily clinical use. Recently, the first studies about corneal nerve imaging using OCT have been reported showing sub-basal nerves and occasional nerves in the stroma.[28–30,39] Most of these studies are proof-of-concept investigations and the image quality clearly lacks the standards of IVCM. Our article presents 3D nerve distribution, 3D nerve tracking, and a one-to-one comparison of the nerves to immunohistochemistry staining, which has not been shown in any of these articles.

Thus, OCT's advantageous characteristics, such as high-speed volumetric data acquisition, noncontact imaging, and scalable FoVs, might enable it to become a convenient clinical alternative to IVCM for corneal nerve imaging.

The future aim to image in vivo with micrometer resolution will face the challenge of the motion of the eye, resulting in motion artifacts. Besides the movements of the animal or patient, the ocular pulse amplitude,[40] which produces small deformations within the ocular tissues including the corneoscleral shell, needs to be considered. However, several successful in vivo OCT imaging studies of the cornea have

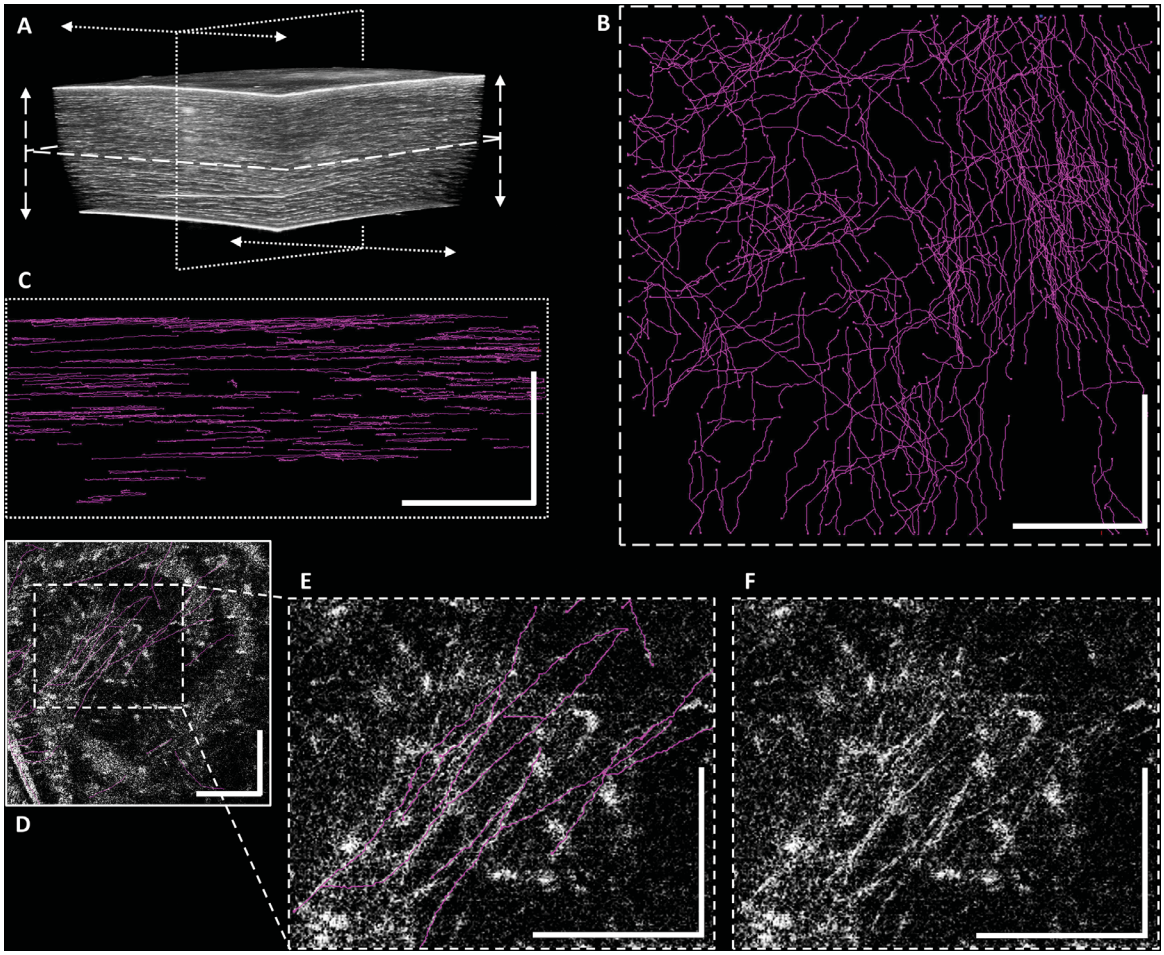

Fig. 3. Representative imaging results of corneal nerve tracking. (A) Three-dimensional rendered volume dataset indicating respective projection planes of (B) and (C). (B) En face plane nerve trace skeleton of semiautomatic tracking procedure (integrated over entire corneal thickness). (C) Cross-sectional plane nerve trace skeleton of semiautomatic tracking procedure (integrated over entire lateral extension of scan). (D) Single representative en face plane indicating traced nerve structures (overlaid in magenta). (E) Zoom in of (D), providing a close up of the tracking procedure (nerve structures overlaid in magenta). (F) Same regions of interest as (E), enabling a comparison with untracked raw intensity en face plane. Scale bar = 250 µm.

been reported previously.[24,28,30] To obtain good in vivo image quality, there will be a need to incorporate dynamic tracking and postprocessing algorithms for reconstruction of the images and to provide high acquisition rates.

One limitation of µOCT for corneal nerve tracking using image segmentation is its intrinsic lack of nerve-specific contrast, in particular within the stroma, where keratocytes and collagen fibrils intertwine with nerval structures. In addition, OCT speckle further degrades image quality. Therefore, fully automated tracking algorithms were insufficient for this investigation, and a semiautomatic algorithm operated by an expert reader was required. However, for certain nerve plexuses with low scattering surroundings, such as the sub-basal plexus, the first fully automated two-dimensional computational nerve segmentation was recently reported.[41] Furthermore, the focus of this study was on imaging the stromal nerves, so no epithelial nerves or the endothelial cells are presented. To reliably judge the corneal state, the size of the volume presented by µOCT could already be sufficient. If a greater volume is needed to determine a clinically useful mean nerve density, increasing the volume is possible. A higher imaging speed, for example by a higher rate of A-scans, should allow for the imaging of larger areas in a clinically acceptable amount of time. Furthermore, imaging of several areas could be performed to reach a more accurate measurement of the mean density of nerves. The creation of larger images could be accomplished by guided imaging and stitching together of several neighboring corneal areas. The required size,

amount, and locations of those areas are currently under investigation.

The possibility of corneal nerve delineation has an impact on many diseases, other than diabetes. Neurotrophic keratopathy is known as a decrease or absence of corneal sensitivity owing to any impairment of the trigeminal nerve. Denervation causes a decrease in epithelial vitality and has an impact on the permeability and wound healing, which can lead to epithelial breakdown, persistent epithelial defects, and stromal ulceration.[42,43] Further etiologies of neurotrophic keratopathy are infections like herpes keratitis, which causes, as one of the most frequent diseases, nerve loss and decreased nerve function,[44,45] and acanthamoeba keratitis with cysts, nerval changes, and radial keratoneuritis[46–48] or status post laser-assisted in situ keratomileusis surgery.[49] In addition, nerve density plays a role in corneal sensation and tear film production.[50,51] Corneal denervation can lead to dry eye, which affects a large amount of the general population.[52] Future studies will aim to quantify morphologic parameters, such as nerval length and density, with the µOCT to compare them among healthy and diseased corneas because these parameters have been shown to be associated with nerve degeneration.[21] Furthermore, in vivo investigations using µOCT will potentially enable to study early onsets of nerval degeneration caused by ophthalmic as well as nonophthalmic diseases.[1–5]

In conclusion, we have presented 3D µOCT corneal nerve imaging and tracking results. The combination of high-resolution imaging, fast data acquisition, scalable FoVs, and noninvasiveness merit further investigations of this technique as a potential future tool for corneal nerve assessment, monitoring, and clinical decision making.

Acknowledgments

Supported by the Wellman Center for Photome dicine Discovery Fund.

Disclosure: **C. Elhardt**, None; **C.M. Wertheimer**, German Research Foundation Research Fellowship (F); **A. Wartak**, SPIE (The International Society for Optics and Photonics) Franz Hillenkamp Fellowship (F); **J. Zhao**, None; **H.M. Leung**, None; **S.A. Kassumeh**, None; **B. Yin**, None; **G.J. Tearney**, Vertex (F), CNUSA Biotech Holdings (F), Astra Zeneca (F), WayVector (F); **R. Birngruber**, None

* CMW and AW are second authors and contributed equally.

** GJT and RB are senior authors and contributed equally.

References

1. Martyn CN, Hughes RA. Epidemiology of peripheral neuropathy. *J Neurol Neurosurg Psychiatry*. 1997;62:310–318.
2. Said G. Diabetic neuropathy–a review. *Nature Clin Pract Neurol*. 2007;3:331–340.
3. Callaghan BC, Cheng HT, Stables CL, Smith AL, Feldman EL. Diabetic neuropathy: clinical manifestations and current treatments. *Lancet Neurol*. 2012;11:521–534.
4. Vernino S, Low PA, Fealey RD, Stewart JD, Farrugia G, Lennon VA. Autoantibodies to ganglionic acetylcholine receptors in autoimmune autonomic neuropathies. *N Engl J Med*. 2000;343:847–855.
5. Chance PF, Alderson MK, Leppig KA, et al. DNA deletion associated with hereditary neuropathy with liability to pressure palsies. *Cell*. 1993;72:143–151.
6. Galer BS, Gianas A, Jensen MP. Painful diabetic polyneuropathy: epidemiology, pain description, and quality of life. *Diabetes Res Clin Pract*. 2000;47:123–128.
7. Jia X, Wang X, Wang X, et al. In vivo corneal confocal microscopy detects improvement of corneal nerve parameters following glycemic control in patients with type 2 diabetes. *J Diabetes Res*. 2018;2018:8516276.
8. Malik RA, Kallinikos P, Abbott C, et al. Corneal confocal microscopy: a non-invasive surrogate of nerve fibre damage and repair in diabetic patients. *Diabetologia*. 2003;46:683–688.
9. Kallinikos P, Berhanu M, O'Donnell C, Boulton AJ, Efron N, Malik RA. Corneal nerve tortuosity in diabetic patients with neuropathy. *Invest Ophthalmol Vis Sci*. 2004;45:418–422.
10. Watson JC, Dyck PJ. Peripheral neuropathy: a practical approach to diagnosis and symptom management. *Mayo Clin Proc*. 2015;90:940–951.
11. Hossain P, Sachdev A, Malik RA. Early detection of diabetic peripheral neuropathy with corneal confocal microscopy. *Lancet*. 2005;366:1340–1343.
12. Sheikh KA. Non-invasive imaging of nerve regeneration. *Exp Neurol*. 2010;223:72–76.
13. Rangavajla G, Mokarram N, Masoodzadehgan N, Pai SB, Bellamkonda RV. Noninvasive imaging

of peripheral nerves. *Cells Tissues Organs*. 2014;200:69–77.
14. Alam U, Jeziorska M, Petropoulos IN, et al. Diagnostic utility of corneal confocal microscopy and intra-epidermal nerve fibre density in diabetic neuropathy. *PloS One*. 2017;12:e0180175.
15. Muller LJ, Marfurt CF, Kruse F, Tervo TM. Corneal nerves: structure, contents and function. *Exp Eye Res*. 2003;76:521–542.
16. Oliveira-Soto L, Efron N. Morphology of corneal nerves using confocal microscopy. *Cornea*. 2001;20:374–384.
17. Jalbert I, Stapleton F, Papas E, Sweeney DF, Coroneo M. In vivo confocal microscopy of the human cornea. *Br J Ophthalmol*. 2003;87:225–236.
18. Guthoff RF, Zhivov A, Stachs O. In vivo confocal microscopy, an inner vision of the cornea - a major review. *Clin Exp Ophthalmol*. 2009;37:100–117.
19. Edwards K, Pritchard N, Dehghani C, et al. Corneal confocal microscopy best identifies the development and progression of neuropathy in patients with type 1 diabetes. *J Diabetes Complications*. 2017;31:1325–1327.
20. Pritchard N, Edwards K, Russell AW, Perkins BA, Malik RA, Efron N. Corneal confocal microscopy predicts 4-year incident peripheral neuropathy in type 1 diabetes. *Diabetes Care*. 2015;38:671–675.
21. Perkins BA, Lovblom LE, Bril V, et al. Corneal confocal microscopy for identification of diabetic sensorimotor polyneuropathy: a pooled multinational consortium study. *Diabetologia*. 2018;61:1856–1861.
22. Hertz P, Bril V, Orszag A, et al. Reproducibility of in vivo corneal confocal microscopy as a novel screening test for early diabetic sensorimotor polyneuropathy. *Diab Med*. 2011;28:1253–1260.
23. dell'Omo R, Cifariello F, De Turris S, et al. Confocal microscopy of corneal nerve plexus as an early marker of eye involvement in patients with type 2 diabetes. *Diabetes Res Clin Pract*. 2018;142:393–400.
24. Tan B, Hosseinaee Z, Han L, Kralj O, Sorbara L, Bizheva K. 250 kHz, 1.5 micron resolution SD-OCT for in-vivo cellular imaging of the human cornea. *Biomed Opt Exp*. 2018;9:6569–6583.
25. Huang D, Swanson EA, Lin CP, et al. Optical coherence tomography. *Science*. 1991;254:1178–1181.
26. Dubois A, Vabre L, Boccara AC, Beaurepaire E. High-resolution full-field optical coherence tomography with a Linnik microscope. *Appl Optics*. 2002;41:805–812.
27. Liu L, Gardecki JA, Nadkarni SK, et al. Imaging the subcellular structure of human coronary atherosclerosis using micro-optical coherence tomography. *Nat Med*. 2011;17:1010–1014.
28. Mazlin V, Xiao P, Dalimier E, et al. In vivo high resolution human corneal imaging using full-field optical coherence tomography. *Biomed Opt Exp*. 2018;9:557–568.
29. Chen S, Liu X, Wang N, et al. Visualizing micro-anatomical structures of the posterior cornea with micro-optical coherence tomography. *Sci Rep*. 2017;7:10752.
30. Chen YT, Tsai CY, Chiu YK, et al. En face and cross-sectional corneal tomograms using sub-micron spatial resolution optical coherence tomography. *Sci Rep*. 2018;8:14349.
31. Yin B, Chu KK, Liang CP, Singh K, Reddy R, Tearney GJ. muOCT imaging using depth of focus extension by self-imaging wavefront division in a common-path fiber optic probe. *Optics Exp*. 2016;24:5555–5564.
32. Yin B, Hyun C, Gardecki JA, Tearney GJ. Extended depth of focus for coherence-based cellular imaging. *Optica*. 2017;4:959–965.
33. Schneider CA, Rasband WS, Eliceiri KW. NIH Image to ImageJ: 25 years of image analysis. *Nat Methods*. 2012;9:671–675.
34. Longair MH, Baker DA, Armstrong JD. Simple Neurite Tracer: open source software for reconstruction, visualization and analysis of neuronal processes. *Bioinformatics*. 2011;27:2453–2454.
35. Jung Y, Ng JH, Keating CP, et al. Comprehensive evaluation of peripheral nerve regeneration in the acute healing phase using tissue clearing and optical microscopy in a rodent model. *PloS One*. 2014;9:e94054.
36. Scharenberg K. The cells and nerves of the human cornea; a study with silver carbonate. *Am J Ophthalmol*. 1955;40:368–379.
37. Toivanen M, Tervo T, Partanen M, Vannas A, Hervonen A. Histochemical demonstration of adrenergic nerves in the stroma of human cornea. *Invest Ophthalmol Vis Sci*. 1987;28:398–400.
38. Bohn S, Sperlich K, Allgeier S, et al. Cellular in vivo 3D imaging of the cornea by confocal laser scanning microscopy. *Biomed Opt Exp*. 2018;9:2511–2525.
39. Werkmeister RM, Sapeta S, Schmidl D, et al. Ultrahigh-resolution OCT imaging of the human cornea. *Biomed Opt Exp*. 2017;8:1221–1239.
40. Perkins E. The ocular pulse. *Curr Eye Res*. 1981;1:19–24.
41. Hosseinaee Z, Tan B, Kralj O, et al. Fully automated corneal nerve segmentation algorithm for corneal nerves analysis from UHR-OCT images. *Ophthalmic Technologies XXIX: International*

Society for Optics and Photonics. 2019;10858: 23.
42. Ferrari G, Chauhan SK, Ueno H, et al. A novel mouse model for neurotrophic keratopathy: trigeminal nerve stereotactic electrolysis through the brain. *Invest Ophthalmol Vis Sci*. 2011;52:2532–2539.
43. Beuerman RW, Schimmelpfennig B. Sensory denervation of the rabbit cornea affects epithelial properties. *Exp Neurol*. 1980;69:196–201.
44. Hamrah P, Cruzat A, Dastjerdi MH, et al. Corneal sensation and subbasal nerve alterations in patients with herpes simplex keratitis: an in vivo confocal microscopy study. *Ophthalmology*. 2010;117:1930–1936.
45. Muller RT, Abedi F, Cruzat A, et al. Degeneration and regeneration of subbasal corneal nerves after infectious keratitis: a longitudinal in vivo confocal microscopy study. *Ophthalmology*. 2015;122:2200–2209.
46. Kurbanyan K, Hoesl L, Schrems W, Hamrah P. Corneal nerve alterations in acute Acanthamoeba and fungal keratitis: an in vivo confocal microscopy study. *Eye*. 2012;26:126.
47. Pfister DR, Cameron JD, Krachmer JH, Holland EJ. Confocal microscopy findings of Acanthamoeba keratitis. *Am J Ophthalmol*. 1996;121:119–128.
48. Yamazaki N, Kobayashi A, Yokogawa H, et al. In vivo imaging of radial keratoneuritis in patients with Acanthamoeba keratitis by anterior-segment optical coherence tomography. *Ophthalmology*. 2014;121:2153–2158.
49. Shtein RM. Post-LASIK dry eye. *Exp Rev Ophthalmol*. 2011;6:575–582.
50. Benitez-Del-Castillo JM, Acosta MC, Wassfi MA, et al. Relation between corneal innervation with confocal microscopy and corneal sensitivity with noncontact esthesiometry in patients with dry eye. *Invest Ophthalmol Vis Sci*. 2007;48:173–181.
51. Labbe A, Alalwani H, Van Went C, Brasnu E, Georgescu D, Baudouin C. The relationship between subbasal nerve morphology and corneal sensation in ocular surface disease. *Invest Ophthalmol Vis Sci*. 2012;53:4926–4931.
52. Farrand KF, Fridman M, Stillman IO, Schaumberg DA. Prevalence of diagnosed dry eye disease in the United States among adults aged 18 years and older. *Am J Ophthalmol*. 2017;182:90–98.

Supplementary Material

Supplementary Movie S1. Rotating three-dimensional nerve trace skeleton of semiautomatic tracking procedure.